Cellular/Molecular

Alternative Splicing of the $Ca_V1.3$ Channel IQ Domain, a Molecular Switch for Ca^{2+}-Dependent Inactivation within Auditory Hair Cells

Yiru Shen,[1] Dejie Yu,[2] Hakim Hiel,[3] Ping Liao,[1] David T. Yue,[4,5] Paul A. Fuchs,[3] and Tuck Wah Soong[1,2]

[1]Department of Physiology, Yong Loo Lin School of Medicine, National University of Singapore, Singapore 117597, [2]National Neuroscience Institute, Singapore 308443,[3]Cochlear Neurotransmission Laboratory, Center for Hearing and Balance, Department of Otolaryngology, Head, and Neck Surgery, and Center for Sensory Biology, Department of Neuroscience, Johns Hopkins University School of Medicine, Baltimore, Maryland 21205-2195, and Departments of [4]Biomedical Engineering and [5]Neuroscience, Ca^{2+} Signals Laboratory, Johns Hopkins University School of Medicine, Baltimore, Maryland 21205

Native $Ca_V1.3$ channels within cochlear hair cells exhibit a surprising lack of Ca^{2+}-dependent inactivation (CDI), given that heterologously expressed $Ca_V1.3$ channels show marked CDI. To determine whether alternative splicing at the C terminus of the $Ca_V1.3$ gene may produce a hair cell splice variant with weak CDI, we transcript-scanned mRNA obtained from rat cochlea. We found that the alternate use of exon 41 acceptor sites generated a splice variant that lost the calmodulin-binding IQ motif of the C terminus. These $Ca_V1.3_{IQ\Delta}$ ("IQ deleted") channels exhibited a lack of CDI, which was independent of the type of coexpressed β-subunits. $Ca_V1.3_{IQ\Delta}$ channel immunoreactivity was preferentially localized to cochlear outer hair cells (OHCs), whereas that of $Ca_V1.3_{IQfull}$ channels (IQ-possessing) labeled inner hair cells (IHCs). The preferential expression of $Ca_V1.3_{IQ\Delta}$ within OHCs suggests that these channels may play a role in processes such as electromotility or activity-dependent gene transcription rather than neurotransmitter release, which is performed predominantly by IHCs in the cochlea.

Key words: **alternative splicing; calcium channels; L-type calcium channels; splice variant; calcium-dependent inactivation; hair cells**

Introduction

Ca^{2+} influx through voltage-gated calcium channels (VGCCs) supports transmitter release from hair cells (Parsons et al., 1994; Beutner and Moser, 2001; Robertson and Paki, 2002), activates calcium-dependent potassium channels, (Lewis and Hudspeth, 1983; Art and Fettiplace, 1987; Fuchs et al., 1988), and may contribute to voltage-driven electromotility (Brownell et al., 1985). In particular, VGCCs are located specifically close to ribbon synapses of inner hair cells (IHCs), so as to rapidly trigger the great majority of afferent signaling in the mammalian cochlea. In contrast, outer hair cells (OHCs) have few, if any, ribbon synapses but, nonetheless, may rely on VGCCs to modulate baseline membrane potential via calcium-dependent potassium channels and to support voltage-driven electromotility that is necessary for cochlear sensitivity and frequency selectivity (Ospeck et al., 2003).

In all of these contexts, $Ca_V1.3$ channels (Xu and Lipscombe, 2001) prevail as the dominant isoform. Evidence for the predominance of $Ca_V1.3$ includes the cloning of $\alpha_1 1.3$ from vertebrate cochlea (Kollmar et al., 1997a,b) and the >90% reduction of Ca^{2+} currents in cochlear hair cells from $Ca_V1.3$ knock-out mice (Platzer et al., 2000). Although, part of the ubiquitous L-type class of Ca^{2+} channels, the subset of $Ca_V1.3$ channels, appears exquisitely specialized for the functional requirements of hair cells. $Ca_V1.3$ channels activate at comparatively negative potentials (Xu and Lipscombe, 2001), fitting with the hyperpolarized operating range of calcium current in native hair cells (Art and Fettiplace, 1987; Hudspeth and Lewis, 1988; Fuchs et al., 1990; Zidanic and Fuchs, 1995; Rodriguez-Contreras and Yamoah, 2001; Xu and Lipscombe, 2001). $Ca_V1.3$ channels exhibit strikingly rapid (de)activation, which permits high-fidelity spike encoding of acoustic stimuli (Zidanic and Fuchs, 1995; Helton et al., 2005). Most intriguingly, the inactivation of $Ca_V1.3$ channels by elevated intracellular Ca^{2+} [Ca^{2+}-dependent inactivation (CDI)] appears weak to absent (Platzer et al., 2000; Michna et al., 2003; Song et al., 2003), in a manner believed to be important for continued perception of sustained auditory signaling (Lewis and Hudspeth, 1983; Glossmann et al., 1987). In contrast, the unmistakable CDI manifest by prototypic L-type channels ($Ca_V1.2$) (Yue and Marban, 1990) emphasizes the specialization of $Ca_V1.3$ properties for hair-cell function. Overall, these customized gating properties may allow $Ca_V1.3$ channels to control tonic neurotransmitter release in hair cells (Fuchs, 1996).

This study and its companion (Yang et al., 2006) seek to establish a molecular basis for the reduced CDI of $Ca_V1.3$ channels

Received May 17, 2006; revised Aug. 30, 2006; accepted Aug. 30, 2006.

This work was supported by a grant from the Singapore Biomedical Research Council (T.W.S.), National Institute for Deafness and Other Communication Disorders Grants R01 DC000276 and P30 DC005211 (P.A.F.), and National Institutes of Health Grants R01 MH65531 and R37 HL076795 (D.T.Y.). We thank Gregory Ming Yeong Tan, Mui Cheng Liang, Sung Ying Ying, and Deborah Tan for their excellent technical assistance. We are also grateful to Drs. Diane Lipscombe (for α_{1D}) and Terry P. Snutch (for rat β_{1-4} subunits and rat $\alpha_2\beta$ subunit) for the generous gift of clones.

Correspondence should be addressed to Tuck Wah Soong, Department of Physiology, Yong Loo Lin School of Medicine, National University of Singapore, MD9, 2 Medical Drive, Singapore 117597. E-mail: phsstw@nus.edu.sg.

DOI:10.1523/JNEUROSCI.2093-06.2006

 0270-6474/06/2610690-10$15.00/0

in cochlear hair cells. Although the companion paper reports on a calcium-binding protein (CaBP) mechanism to moderate hair-cell CDI, this report explores how the baseline CDI of $Ca_V1.3$ channels may be switched "off" by alternative splicing of the IQ region on the C terminus of α_1 subunit, resulting in $Ca_V1.3_{IQ\Delta}$ channels that lack CDI. Previously, $Ca_V1.3$ channels encompassing an intact IQ region ($Ca_V1.3_{IQfull}$) have been the focus of functional studies; these channels exhibit CDI commonly associated with recombinant $Ca_V1.3$ channels. Also, we found that $Ca_V1.3_{IQ\Delta}$ channels are substantially enriched in OHCs, whereas IHCs feature a predominance of $Ca_V1.3_{IQfull}$ channels. Thus, alternative splicing may serve to moderate CDI within OHCs specifically.

Materials and Methods

Tissue preparation and distribution of splice variant, $Ca_V1.3_{IQ\Delta}$

All animal protocols were approved by national ethical guidelines. Rat pups (Charles River Laboratories, Wilmington, MA), between postnatal day 9 (P9) (before onset of hearing) and P28 (hearing fully developed) where P0 is the date of birth, were anesthetized using pentobarbital and were decapitated. The cochleas were rapidly removed and the organ of Corti was microdissected for subsequent procedures. For each RNA isolation experiment, two organs of Corti were processed under sterile RNase-free conditions. Total RNA was isolated from the organ of Corti from rat pups of different ages (P9 and P28) with a solution of phenol and guanidinium isothiocyanate (Trizol; Invitrogen, San Diego, CA). First-strand cDNA was synthesized with reverse transcriptase (Superscript II; Invitrogen) and oligo(dT) primers (Invitrogen). Negative control reactions without reverse transcriptase were performed in all reverse transcription (RT)-PCRs to exclude contamination by genomic DNA. For the cDNA first-strand synthesis, each reaction was incubated at 25°C for 10 min, followed by 42°C for 1 h, and the reaction was inactivated at 95°C for 5 min. The cDNA was stored at −20°C until PCR analysis.

Initial PCRs were conducted using rat $Ca_V1.3$-specific primers flanking the IQ region of the $Ca_V1.3$ channel. The following primers were used to amplify a 638 bp stretch of $Ca_V1.3$ subunit around the IQ motif, which was subjected to alternative splicing: sense primer, 5′-ACGGACGGCTCTCAAGATCAAG-3′; antisense primer, 5′-GGGCAGCTTTGGACATATTGG-3′. The PCR protocol includes an initial denaturation step at 95°C for 2 min; five cycles of 95°C for 30 s, step down 60–55°C, stepping down 1°C for each cycle and 72°C for 1 min, and followed by 30 cycles of 95°C for 30 s, 53°C for 30 s, and 72°C for 1 min; and a final extension step at 72°C for 10 min. PCR products were analyzed by agarose gel electrophoresis. The amplicons were subcloned into pGEM-T Easy vector and transformed into DH10B *Escherichia coli* cells. The different splice combinations were differentiated based on their distinct migration patterns in 2% agarose gels. To verify the accuracy of the gel analysis, plasmids extracted from representative colonies were sent for DNA sequencing.

The amplicon containing the splice variant, $Ca_V1.3_{IQ\Delta}$, was cloned into pGEMT-Easy vector (Promega, Madison, WI), and sequences were compared using the Lasergene software (DNAstar, Madison, WI) sequence alignment or against the National Center for Biotechnology Information database. To characterize the functional properties of $Ca_V1.3_{IQ\Delta}$, this splice variant was substituted into the full-length wild-type (WT)-$Ca_V1.3_{IQfull}$ (kindly provided by Dr. Diane Lipscombe, GenBank accession number AY370009) and $Ca_V1.3_{IQ\Delta}$ construct generated. The $Ca_V1.3_{IQ\Delta}$ construct (truncated IQ motif) contains an exon, which is subjected to alternative splicing at the IQ region of $Ca_V1.3$ subunit, thus generating a truncated protein that is different from the $Ca_V1.3_{IQfull}$ (full IQ).

Generation of polyclonal antibody against $Ca_V1.3_{IQ\Delta}$ splice variant and $Ca_V1.3_{IQfull}$

The rat $Ca_V1.3_{IQ\Delta}$ splice variant (GNSRSGKSKAWWGNTLRRTPRSPYRRD) was subcloned in frame between *Eco*RI and *Xho*I sites of the expression plasmid pGEX-4T-1 (GE Healthcare, Arlington Heights, IL). The resulting fusion protein was expressed in the host *Escherichia coli* BL21 (DES). This clone is designed $Ca_V1.3_{IQ\Delta}$-glutathione *S*-transferase (GST). GST-fused $Ca_V1.3_{IQ\Delta}$ protein was purified and eluted with glutathione-agarose (G 4501; Sigma, St. Louis, MO). Purified $Ca_V1.3_{IQ\Delta}$-GST proteins were dialyzed in PBS (137 mM NaCl, 2.7 mM KCl, and 10 mM sodium phosphate, pH 7.4) before being used to immunize female New Zealand White rabbit once a month. Complete Freund's adjuvant (F 5881; Sigma) was first mixed with $Ca_V1.3_{IQ\Delta}$-GST for immunization, and incomplete Freund's adjuvant (F 5506; Sigma) was used in subsequent injections once a month. Serum was preabsorbed overnight at 4°C with excess GST protein to remove contaminating GST IgG in the serum and the polyclonal antibody of interest (pAb_ΔIQ) was affinity-purified from immobilized $Ca_V1.3_{IQ\Delta}$-GST protein with an IgG elution buffer (Pierce, Rockford, IL). Serum from rabbits before immunization was used as preimmune control in Western blot analysis. The synthetic peptide (Genemed Synthesis, South San Francisco, CA) GNSRSGKSKAWWGNTLRRTPRSPYRRD, which represents the region of splice variant, was synthesized and used as preabsorption control. The concentration of the peptide was 40 mg/ml. The concentration of antibody was ~1 μg/μl and was designed as pAb_ΔIQ.

The polyclonal peptide antibody designated as pAb_$Ca_V1.3$ was raised (Alpha Diagnostic International, San Antonio, TX) against exon 42a (6 aa MLERML) and two additional amino acids from exon 41 (LQ). The peptide CLQMLERML was synthesized and used for generation of peptide-antibody against $Ca_V1.3_{IQfull}$ channels in rabbits. The inclusion of an additional residue C (cysteine) is to stabilize and increase the ease of affinity purification of the peptide. The concentration of antibody was ~0.8 μg/μl.

Protein immunoblotting

To get sufficient protein for immunoblotting, 30 whole-rat cochleas (180 mg) were used for each protein extraction. Tissues from the rat cochleas were homogenized in cold lysis buffer containing 50 mM Tris, pH 8.0, 1 mM EDTA, and 150 mM NaCl. All processes were done at 4°C. The homogenate was centrifugated at 8000 rpm for 15 min, followed by 40,000 rpm for 1 h. Membrane proteins were extracted from the pellet with cold lysis buffer supplemented with 1% Triton X-100 for 1 h. Subsequently, the pellet was centrifuged at 40,000 rpm for 1 h. Membrane protein was extracted from the supernatant, and 20 μg of protein was separated in 6% SDS polyacrylamide gel under reducing conditions. The protein was then transferred electrophoretically onto polyvinylidene difluoride membrane (Bio-Rad, Hercules, CA) using a semi-dry transfer system (Bio-Rad), and methanol was omitted from the transfer buffer.

For antibody detection, the membrane was incubated with 5% nonfat milk in TBST (20 mM Tris, pH 7.6, 137 mM NaCl, and 0.05% Tween 20) for 1 h at room temperature. The membrane was then incubated with diluted primary antibody pAb_ΔIQ (used at 1:250) or with diluted primary antibody pAb_$Ca_V1.3$ (used at 1:50) at 4°C overnight. After five washes with TBST, the membrane was incubated for 1 h with diluted 2000-fold goat anti-rabbit secondary antibody (Sigma). After five washes, the specific binding of the primary antibody was detected with SuperSignal Ultra chemiluminescent substrate (Pierce).

Electrophysiological recordings and data analysis

Whole-cell patch-clamp recordings were used to characterize full-length wild-type $Ca_V1.3_{IQfull}$ and its splice variant $Ca_V1.3_{IQ\Delta}$. Ca^{2+} currents were recorded using the whole-cell patch-clamp technique from transiently transfected mammalian human embryonic kidney 293 (HEK293) cells according to methods described previously at room temperature (Patil et al., 1998; Peterson et al., 1999). Outward K^+ currents were blocked by Cs^+ in the internal and external solutions. Mammalian HEK293 cells were transiently transfected either with full-length wild-type $Ca_V1.3_{IQfull}$ or $Ca_V1.3_{IQ\Delta}$, rat β subunits (β_{1b}, β_{2a}, β_3, β_4), and rat $\alpha_2\delta$ subunits using the standard calcium phosphate transfection method. The rat β subunits and rat $\alpha_2\delta$ subunit clones were kindly provided by Dr. Terry P. Snutch (University of British Columbia, Vancouver, British Columbia, Canada). I_{Ca} or I_{Ba} was recorded at room temperature using the whole-cell patch-clamp technique, 48–72 h after transfection. For whole-cell patch-clamp recordings, the internal solution (patch-pipette solution) contained the following (in mM): 138 Cs-MeSO3, 5 CsCl, 0.5

EGTA, 10 HEPES, 1 MgCl2, 2 mg/ml Mg-ATP, pH 7.3 (adjusted with CsOH), 290 mOsm with glucose. The external solution contained the following (in mM): 10 HEPES, 140 tetraethylammonium methanesulfonate, 10 $BaCl_2$, or 10 $CaCl_2$ (pH was adjusted to 7.4 with CsOH and osmolarity to 290–310 with glucose). Pipettes of resistance 1.5–2 MΩ were used. Whole-cell currents, obtained under voltage clamp with an Axopatch 200B amplifier (Molecular Devices, Union City, CA), were filtered at 1–5 kHz and sampled at 5–50 kHz, and the series resistance was typically <5 MÙ after >70% compensation. A P/4 protocol was used to subtract on-line the leak and capacitive transients.

Data were acquired using the software pClamp9 (Molecular Devices) and were analyzed and fitted using Graphpad Prism IV software (San Diego, CA) and Microsoft (Seattle, WA) Excel. Data are expressed as mean values ± SE. Statistical analysis was performed using paired or unpaired Student's *t* test. Current–voltage (*I–V*) curve relationships were obtained by step depolarization from a holding potential of −100 mV to various test potentials. *I–V* curves were fitted according to Equation 1: $I = G_{max}(V - E_{rev})/(1 + \exp[(V - V_{1/2act})/k_{I-V}])$, where G_{max} is the maximum conductance of the cell, E_{rev} is the reversal potential, $V_{½act}$ is the voltage for half-maximal activation, k_{I-V} is the slope factor of Boltzmann function, and *n* is the number of tested cells. Steady-state inactivation (SSI) data and CDI were fitted to Equation 2: $amp_1 + (1 - amp_1)/(1 + \exp[(V - V_{1/2inact})/SF1]) + amp_2/(1 + \exp[-(V - V'_{1/2inact})SF2]$, where amp_1 is the initial current amplitude, amp_2 is the final current amplitude, *V* is the membrane potential of the conditioning pulse, $V_{½inact}$ is the potential for half-inactivation, and SF is the slope factor.

Immunocytochemistry

Whole-mount tissues. Whole cochleas were dissected from rat pups and immediately perfused through the round window with ice-cold 2% paraformaldehyde (PFA) buffered with 0.1 M monobasic sodium phosphate, 0.1 M L-lysine hydrochloride and 0.01 M periodic acid, pH 7.4. Cochleas were allowed to fix in 2% PFA buffered with 0.1 M monobasic sodium phosphate for 2–3 h before being rinsed with fresh 0.1 M phosphate buffer. All incubation and rinsing steps are performed on a rocking table. The organ of Corti was excised from the cochleas and blocked in blocking buffer (60 mM PBS with 5% normal goat serum and 0.25% Triton X-100) for 1 h at room temperature. The primary antibody was diluted in blocking buffer, and the organ of Corti was incubated overnight at 4°C. Thereafter, it was rinsed in blocking buffer twice before incubating with secondary antibody for 2 h at room temperature. The organ of Corti was rinsed twice in PBS (60 mM PBS with 0.25% Triton X-100) before mounting on glass slides with FluorSave mounting medium (Chemicon, Temecula, CA).

Frozen sections. Rat pups of various ages (P9 and P28) were used for these experiments. Immediately after decapitation, the excess bones were dissected away, and the whole cochleas were perfused with ice-cold 2% paraformaldehyde buffered with 0.1 M monobasic sodium phosphate, 0.1 M L-lysine hydrochloride, and 0.01 M periodic acid, pH 7.4. After fixation for 3 h, excess bones and connective tissues were removed, and the organs of Corti were decalcified for up to 72 h at 4°C in 5% EDTA buffered with 0.1 M phosphate buffer. After several rinses (1–3 h each) with fresh 0.1 M phosphate buffer, the tissue samples were saturated with 30% sucrose in 0.1 M phosphate buffer overnight at 4°C before serial-sectioned. The cochleas were embedded in OCT compound, frozen quickly with liquid nitrogen, and readied for serial sections at −25°C. Fourteen-micrometer-thick cochlear sections were collected by cyrosection and layered on Superfrost slides (Fisher Scientific, Hampton, NH). The slides were coated with poly-lysine before use. The slides were dried at 60–70°C on a slide warmer and stored with desiccant at −20°C until use.

Cochlear sections were thawed and warmed at 37°C for 20 min before antibody exposure. The sections were first permeabilized and preblocked with blocking buffer (60 mM PBS with 5% normal goat serum and 0.25% Triton X-100) for 1 h at room temperature. The primary antibody, pAb_ΔIQ raised in rabbit, was diluted 1:200 in blocking buffer and incubated overnight at 4°C in a humid chamber. When the primary antibody, pAb_$Ca_V1.3$, was used, the antibody was diluted at 1:50 in blocking buffer and incubated overnight at 4°C. To observe afferent fiber innervation, anti-NF200 (mouse monoclonal, clone 52, N0142, 1:1000; Sigma) was used. Thereafter, it was rinsed in blocking buffer twice before incubating with diluted 1:8000 secondary antibody (goat anti-rabbit Alexa Fluor 488-conjugated antibodies and goat anti-mouse Alexa Fluor 594-conjugated antibodies; Invitrogen) for 2 h at room temperature. The sections were rinsed twice in PBS (60 mM PBS with 0.25% Triton X-100) before mounting on glass slides with FluorSave mounting medium (Chemicon).

To test for nonspecific staining, preabsorption controls were performed by incubating the primary antibody, pAb_ΔIQ, with a concentrated solution of GST protein (25 μM) and synthetic peptide (at concentration of 40 μg/μl; Genemed Synthesis, South San Francisco, CA) for 2 h at room temperature. The molar ratio of blocking peptide to antibody was 100:1. Solutions were then spun at 12,000 rpm for 5 min at 4°C before diluting to the final working concentration to be used on the sections. For preabsorption controls of polyclonal peptide antibody, pAb_$Ca_V1.3$, 2 μg/μl of the commercially provided fusion protein was used.

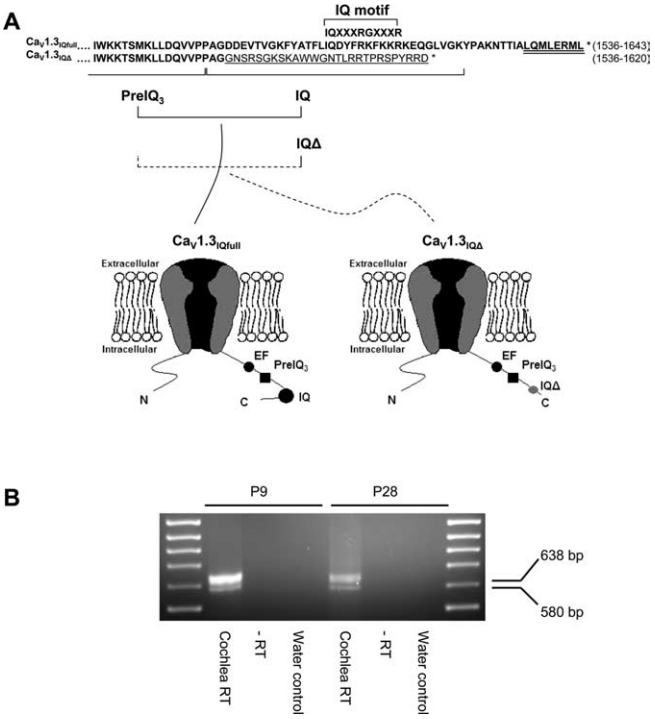

Figure 1. Schematic representation of alternative splicing of $Ca_V1.3$ IQ motif at C terminus. ***A***, Top, Alignment of partial amino acid sequences of C-terminal regions of $Ca_V1.3_{IQfull}$ and $Ca_V1.3_{IQΔ}$ subunits. The deleted IQ domain as replaced by novel amino acid residues in the C terminal end are represented by gray letters, and these underlined residues were part of the GST fusion protein used to raise pAb_ΔIQ. The 8 aa (underlined doubly) downstream of the IQ motif in $Ca_V1.3_{IQfull}$ channels were used to raise the peptide antibody, pAb_$Ca_V1.3$. Bottom, Left, Diagram of $Ca_V1.3_{IQfull}$ channel containing the EF hand, $PreIQ_3$, and IQ domains. Right, Diagram of $Ca_V1.3_{IQΔ}$ channel showing EF hand and $PreIQ_3$ are preserved, but the IQ domain is deleted. ***B***, Agarose gel shows two PCR amplicons (638 and 580 bp) representing two splice variants derived from alternate use of acceptor sites of exon 41. Lane 1, mRNA from P9 cochlea; lane 4, mRNA from P28 cochlea; lanes 2, 3, 5, and 6, negative controls.

Results

Transcript scanning of $Ca_V1.3$ mRNA from auditory hair cells

To explore whether alternative splicing of $Ca_V1.3$ channels might explain the diminished CDI characteristic of native channels in hair cells, we applied "transcript-scanning" (Soong et al., 2002) to the principal α_1 subunit of $Ca_V1.3$ channels. We focused on the C terminus of $Ca_V1.3$ (Fig. 1*A*), because the analogous region of homologous $Ca_V1.2$ channels contains important structural determinants for the CDI of the latter channels (Peterson et al., 2000). Transcript-scanning enabled a systematic search for splice

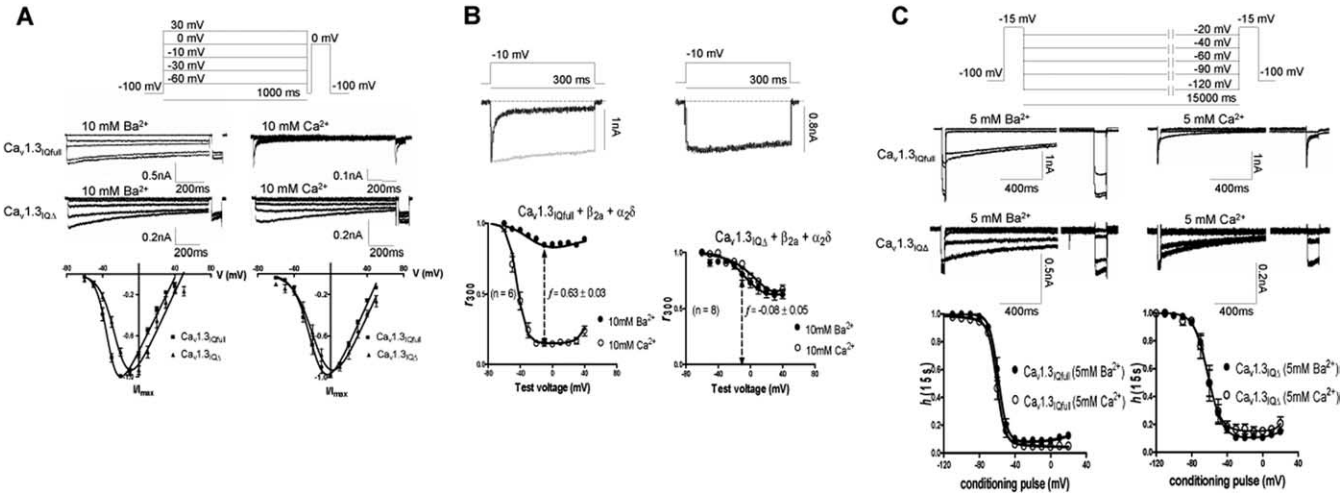

Figure 2. Voltage-dependent electrophysiological properties of splice variants. ***A***, Top, Exemplar current traces of $Ca_V1.3_{IQfull}$ and $Ca_V1.3_{IQ\Delta}$ channels evoked by test pulses that were stepped from holding potential of −100 mV to −60, −30, −10, 0, 30 mV for 1 s. Left, A family of whole-cell *I–V* relationships of $Ca_V1.3_{IQfull}$ and $Ca_V1.3_{IQ\Delta}$ channel recordings performed in Ba^{2+} (left) or Ca^{2+} (right). Both $Ca_V1.3_{IQfull}$ (■) and $Ca_V1.3_{IQ\Delta}$ (▲) channels were cotransfected with auxiliary subunits (β_{2a} and $\alpha_2\delta$) in mammalian HEK293 cells, and the average *I–V* relationships were obtained by fitting with the equation $I = G_{max}(V - E_{rev})/\{1 + \exp[(V - V_{½act})/k_{I-V}]\}$, where G_{max} is the maximum conductance of the cell, E_{rev} is the reversal potential, $V_{½act}$ is the voltage for half-maximal activation, k_{I-V} is the slope factor of Boltzmann function, and *n* is the number of cells. $V_{½act}$ values from peak *I–V* plots of $Ca_V1.3_{IQfull}$ and $Ca_V1.3_{IQ\Delta}$ channels in 10 mM barium are -33.42 ± 0.67 mV ($n = 9$) and -23.54 ± 1.54 mV ($n = 9$), respectively; and in 10 mM Ca^{2+}, the $V_{½act}$ values are -18.76 ± 1.25 mV ($n = 8$) and -13.83 ± 2.33 mV ($n = 8$), respectively. ***B***, Robust CDI exhibited by $Ca_V1.3_{IQfull}$ channels, and weak CDI was observed for $Ca_V1.3_{IQ\Delta}$ channels. Open and closed circles indicate the relationships with Ba^{2+} and Ca^{2+} as charge carrier, and the *f* value is an index of pure CDI obtained as a difference between Ba^{2+} and Ca^{2+} r_{300} relationships at −10 mV. The difference in *f* values is statistically significant ($p < 0.01$). ***C***, SSI properties of $Ca_V1.3_{IQfull}$ and $Ca_V1.3_{IQ\Delta}$ channels. Top, A family of exemplar current traces after 15 s conditioning depolarizing pulses evoked at −120, −90, −60, −40, or −20 mV of both $Ca_V1.3_{IQfull}$ and $Ca_V1.3_{IQ\Delta}$. Bottom, Graphs of SSI, hours (15 s), as a function of conditioning pulses obtained from normalized data points. Steady-state inactivation was fitted with the equation $amp_1 + (1 - amp_1)/(1 + \exp[(V - V_{½inact})/SF1]) + amp_2/(1 + \exp[-(V - V'_{½inact})/SF2])$, where amp_1 is initial current amplitude, amp_2 is final current amplitude, *V* is the membrane potential of the conditioning pulse, $V_{½inact}$ is the potential for half-inactivation, and *SF* is the slope factor. The $V_{½inact}$ of wild-type $Ca_V1.3_{IQfull}$ and splice variant $Ca_V1.3_{IQ\Delta}$ channels are as follows: 5 mM barium, -58.79 ± 4.98 mV ($n = 10$) and -61.39 ± 7.76 mV ($n = 10$), respectively.

variations, including regions surrounding the IQ domain of the $Ca_V1.3$ subunit. In the course of this scan, we found an unusual splice variant at exon 41, in which the IQ motif was essentially deleted, and other unrelated residues were substituted (Fig. 1*A*). Specifically, we used exon-specific primers flanking the IQ segment of the $Ca_V1.3$ subunit to amplify mRNA transcripts isolated from the organ of Corti, as dissected from 9 and 28 d postnatal rats (P9 and P28). Two amplicons of 638 and 580 bp in length were visualized. DNA sequencing of the smaller PCR product revealed a deletion of 58 bp that encodes the 5′-half of the IQ motif (Fig. 1*B*). Interestingly, the alternative use of the exon 41 acceptor site also frame-shifted the remaining 3′-half of exon 41, resulting in the addition of 27 unrelated amino acids after exon 40, followed by a premature stop TAG at nucleotide position 5419. Examination of the genomic sequence of the $Ca_V1.3$ subunit (NW_043030.1; GenInfo, 26008970) suggests that alternative splicing at exon 41 uses canonical GU-AG splice donor and acceptor sites. Essentially, alternative splicing at exon 41 removed the entire IQ domain of the $Ca_V1.3$ channel to form a novel splice variant (yielding channels with the designation $Ca_V1.3_{IQ\Delta}$). The more commonly recognized $Ca_V1.3$ channels, those with $Ca_V1.3$ subunits containing a full IQ domain (Xu and Lipscombe, 2001), will henceforth be referred to as $Ca_V1.3_{IQfull}$ channels [equivalent to channels containing α_{1Dsh} (Yang et al., 2006)].

$Ca_V1.3_{IQ\Delta}$ channels lack Ca^{2+}-dependent inactivation

Because calmodulin (CaM) interactions with the IQ motif of many Ca_V1–2 channels mediate CDI (Liang et al., 2003), we hypothesized that the IQ deletion in $Ca_V1.3_{IQ\Delta}$ channels might also exhibit loss of CDI. Alternatively, these channels might altogether fail to express at the surface membrane, because CaM/IQ interactions may be important for proper targeting of channels (Gao et al., 2000). To test for these possibilities, we transfected $Ca_V1.3_{IQ\Delta}$ channels into mammalian HEK293 cells with rat β_{2a} subunits and rat $\alpha_2\delta$ auxiliary subunits (Peterson et al., 1999). Although diminished somewhat in amplitude compared with $Ca_V1.3_{IQfull}$ channels, $Ca_V1.3_{IQ\Delta}$ channels nevertheless supported appreciable current (Fig. 2*A*). Ba^{2+} current waveforms were similar between the two channel types (top left), as were peak current versus voltage (*I–V*) relationships, obtained with either Ba^{2+} or Ca^{2+} as charge carrier (bottom).

In contrast, closer examination of the exemplar Ca^{2+} current waveforms for the two channels (top right) revealed a striking contrast in behavior. Although $Ca_V1.3_{IQfull}$ Ca^{2+} currents showed pronounced inactivation during step depolarization [consistent with the strong CDI characterized in the study by Yang et al. (2006)], such CDI was notably reduced in currents through $Ca_V1.3_{IQ\Delta}$ channels. Figure 2*B* further characterizes this contrast in CDI. Exemplar traces at the top, displayed on a faster time base, re-emphasize the contrasting CDI profiles of the two channel types. More quantitatively, the fraction of peak Ca^{2+} current remaining after 300 ms depolarization (r_{300}) showed a deep U-shape for $Ca_V1.3_{IQfull}$ channels, consistent with strong CDI. In contrast, the analogous relationship for $Ca_V1.3_{IQ\Delta}$ channels exhibited only a shallow decline, no different than with Ba^{2+} as charge carrier. This similarity is consistent with a complete elimination of CDI. For Ba^{2+} currents, they decayed little during 1 s step depolarizations (Fig. 2*A*, top left), consistent with sparse voltage-dependent inactivation (VDI) mechanisms in both cases (Fig. 2*B*, shallow r_{300} relationships). It follows that a convenient index of pure CDI could be specified by an *f* value index, calculated as the difference in r_{300} measured in Ca^{2+} and Ba^{2+} at −10 mV (Peterson et al., 1999; DeMaria et al., 2001). The reduction of

f from ~0.6 to 0 quantifies the elimination of CDI in $Ca_V1.3_{IQ\Delta}$ channels. Steady-state inactivation properties, mainly reflective of voltage-dependent inactivation, were identical between the two types of channels, whether Ba^{2+} or Ca^{2+} was used as the charge carrier (Fig. 2*C*). Hence, $Ca_V1.3_{IQ\Delta}$ channels not only expressed but demonstrated selective loss of CDI.

Elimination of CDI in $Ca_V1.3_{IQ\Delta}$ channels is independent of β-subunit isoform

It is well known that different auxiliary β subunit isoforms can produce different voltage-dependent inactivation (Cens et al., 2006). To determine whether the amount of CDI experienced by $Ca_V1.3_{IQ\Delta}$ and $Ca_V1.3_{IQfull}$ channels might be influenced by the type of β-subunit present, we explicitly characterized both channel types during coexpression with various rat β-subunits (other than the rat β_{2a} already used in Fig. 2). For $Ca_V1.3_{IQfull}$ channels, the extent of VDI was only modestly affected by the choice of β subunit (Fig. 3*A–C*), whereas the CDI was essentially unchanged. Likewise, for $Ca_V1.3_{IQ\Delta}$ channels, voltage-dependent inactivation showed only mild dependence on the β subunit present, and CDI was uniformly weak to absent, with $f < 0.1$ throughout (Fig. 3*D–F*). Overall, these results indicate that the elimination of CDI seen in the $Ca_V1.3_{IQ\Delta}$ channel splice variant is likely independent of the choice of auxiliary β subunit. Here, we calculated the normalized VDI, r_{300} at 300 ms for different rat b subunits (Fig. 4). When we compared the normalized VDI for all β-subunits coexpressing with $Ca_v1.3_{IQ\Delta}$ (Fig. 4*A*) or $Ca_v1.3_{IQfull}$ channels (Fig. 4*B*) with respect to β_{2a}, we found that the effects of both β_{1b} and β_3 on VDI were significantly different (Student's *t* test; $p < 0.001$) but not when β_4 (Student's *t* test; $p > 0.05$) was used. We concluded that the splice variant $Ca_v1.3_{IQ\Delta}$ channels did not display much difference in VDI when we compared with $Ca_v1.3_{IQfull}$ channels for each coexpressing species of β-subunit. Together, our data suggest that alternative splicing at the IQ motif appears to have a prominent effect on CDI with little or no effect on VDI.

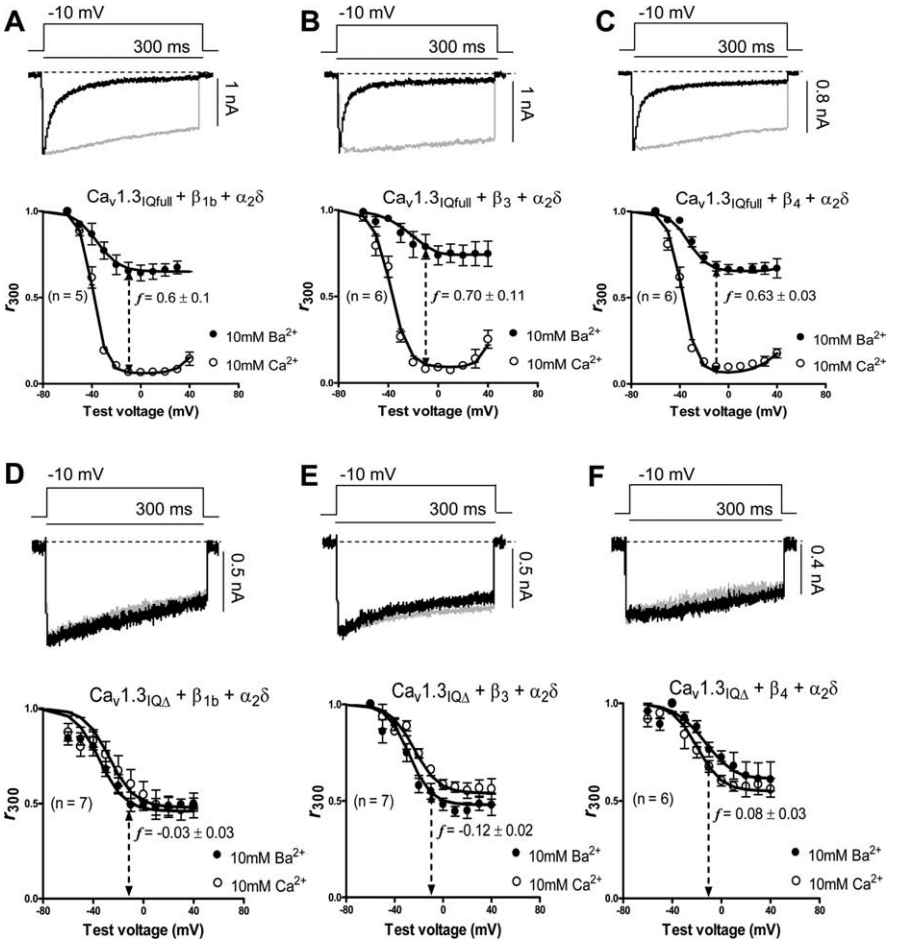

Figure 3. Coexpression of $Ca_V1.3_{IQfull}$ with different β-subunits shows robust CDI, but coexpression with $Ca_V1.3_{IQ\Delta}$ channels lacks CDI. ***A–C***, The index of CDI is quantified by plotting the ratio of remaining current at the end of 300 ms depolarization at different membrane potentials, as a fraction of initial peak current (r_{300}) averaged from $n = 5$ or 6 cells. Open and closed circles indicate the relationships with Ba^{2+} and Ca^{2+} as charge carrier, and the *f* value is an index of pure CDI obtained as a difference between Ba^{2+} and Ca^{2+} r_{300} relationships at −10 mV. CDI reaches its peak, thus producing a typical U-shaped inactivation curve, when recorded in Ca^{2+} and is absent when replaced with Ba^{2+}. Representative current traces show normalized I_{Ca} (black) and I_{Ba} (gray) during a 300 ms depolarization step to +40 mV from a holding potential of −90 mV. Results were obtained for I_{Ca} (○) and I_{Ba} (●) from mammalian HEK293 cells transfected with $Ca_V1.3_{IQfull}$ and the different auxiliary subunits (β_{1-4} and $\alpha_2\delta$). The *f* values represent the mean ± SEM. ***D–F***, Family of CDI obtained from $Ca_V1.3_{IQ\Delta}$ channels in combinations with different β-subunits. The analyses and format are identical to that of ***A–C***. The data are averaged from $n = 6–8$ cells showing distinct loss of CDI. No significant difference ($p > 0.05$) was observed within the group of different β-subunits coexpression $Ca_V1.3_{IQ\Delta}$ or $Ca_V1.3_{IQfull}$ channels in mammalian HEK293 cells. The *f* values represent the mean ± SEM.

Characterization of pAb_ΔIQ and pAb_Ca_v1.3-specific antibodies

At this point, explicit localization of $Ca_V1.3_{IQ\Delta}$ channels within hair cells was a key remaining uncertainty. Also, the splice variant-specific expression of the $BK_{(Ca)}$ channels along the tonotopic gradient of the basilar membrane of the cochlea (Jiang et al., 1997; Navaratnam et al., 1997; Rosenblatt et al., 1997; Jones et al., 1998) made us wonder whether an analogous spatial pattern of $Ca_V1.3_{IQ\Delta}$ expression might also be present. We therefore raised specific polyclonal antibodies against the $Ca_V1.3_{IQ\Delta}$ and $Ca_V1.3_{IQfull}$ channels. For $Ca_V1.3_{IQ\Delta}$, there are 27 amino acids that are not found in $Ca_V1.3_{IQfull}$ channels (Fig. 1); these arise from the frame-shift produced by the alternate use of the acceptor site from exon 41. A polyclonal antibody was thereby generated against a GST fusion to this 27 amino acid sequence, yielding antibody pAb_ΔIQ. For $Ca_V1.3_{IQfull}$ channels, a polyclonal peptide antibody was raised (Alpha Diagnostic International) (described in Materials and Methods against exon 42a; GenBank accession number AF370010), which encodes eight amino acids downstream of the IQ motif (present in $Ca_V1.3_{IQfull}$ but not in $Ca_V1.3_{IQ\Delta}$) (Fig. 1). The resulting antibody was denoted as pAb_Ca_V1.3. In both cases, antibodies were affinity purified before use.

To establish the specificity of pAb_ΔIQ, we were able to stain mammalian HEK293 cells coexpressing $Ca_V1.3_{IQ\Delta}$ channels (labeled red with rhodamine-conjugated anti-rabbit IgG) with β_{2a} subunits (GFP-tagged) (Fig. 5*Ai*) but not those expressing $Ca_V1.3_{IQfull}$ channels (Fig. 5*Aii*). We decided to perform another test to determine the specificity of pAb_ΔIQ on channels ex-

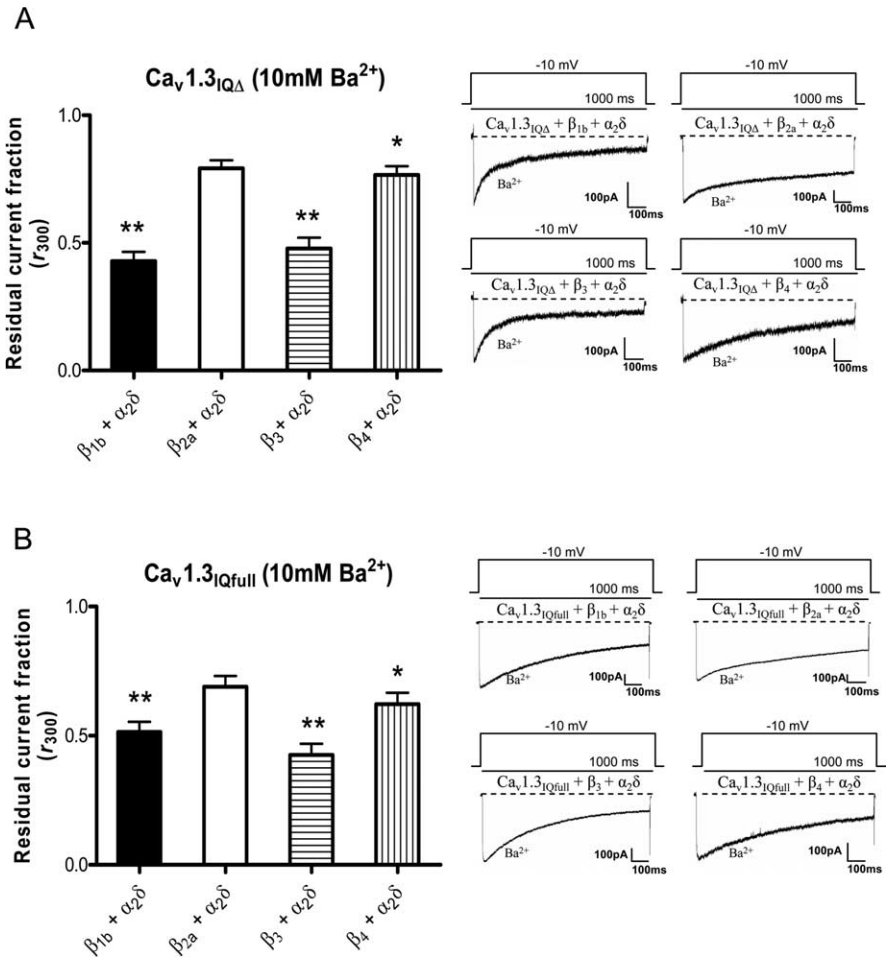

Figure 4. Alternative splicing at the IQ motif affect VDI in $Ca_V1.3_{IQ\Delta}$ channels. Left, Graphical representation of residual fractions of peak currents remaining after a 300 ms test pulse (r_{300}) plotted for the different rat β subunits with $Ca_V1.3_{IQ\Delta}$ (***A***) and $Ca_V1.3_{IQfull}$ (***B***) channels ($n = 8–13$ cells). Right, Exemplar current traces for $Ca_V1.3_{IQ\Delta}$ (top right) and $Ca_V1.3_{IQfull}$ (bottom right) with different rat β subunits recorded at peak current for a 1 s depolarizing step at -10 mV. We calculated the normalized VDI, r_{300} (I_{300}/I_{peak}), at 300 ms for different β subunits. Compared with β_{2a}, $^{**}p < 0.001$ significantly different, $^{*}p > 0.05$ not significantly different (Student's *t* test).

pressed in HEK293 cells. We found strong immunolabeling of the $Ca_V1.3_{IQ\Delta}$ transfected HEK293 cells (red) by commercial anti-$Ca_V1.3$ antibody (Alomone Labs, Jerusalem, Israel). This result indicated that pAb_ΔIQ has indeed immunolabeled a $Ca_V1.3$ splice variant (Fig. 5*Aiii*). Conversely, pAb_$Ca_V1.3$ selectively stained cells (red) expressing $Ca_V1.3_{IQfull}$ channels (Fig. 5*Aiv*) but not those expressing $Ca_V1.3_{IQ\Delta}$ channels (Fig. 5*Av*).

For coarse detection of both of these channels within the entire rat cochlea, we performed Western blot analyses on whole cochlear protein lysates, and both antibodies detected ~180 kDa bands, corresponding to the predicted molecular weights of these channel types [$\alpha_{1D\text{-}IQ\Delta}$ for $Ca_V1.3_{IQ\Delta}$ (Fig. 5*B*, lane 1) and $\alpha_{1D\text{-}IQfull}$ for $Ca_V1.3_{IQfull}$ (Fig. 5*B*, lane 2)].

Selective localization of $Ca_V1.3_{IQ\Delta}$ and $Ca_V1.3_{IQfull}$ channels within cochlear hair cells

Having established the selectivity of these antibodies, we performed immunolabeling on cochlear sections and whole mounts. In the adult organ of Corti (P28), we found that pAb_ΔIQ ($Ca_V1.3_{IQ\Delta}$ channels) labeled all three rows of the OHCs intensely, whereas the IHC showed only weak labeling (Fig. 6*AI*) as shown for the basal turn (BT). An overall sense of the distribution of presumed $Ca_V1.3_{IQ\Delta}$ channels in OHCs is given by the whole-mount section shown in (Fig. 6*AII*). This pattern of OHC labeling was primarily conserved in more basal sections of the organ of Corti, with a hint of lessened labeling in the most apical turns (Fig. 6*BI–BIII*). For orientation, anti-NF200 (red) specifically labeled afferent fibers that innervate the synaptic region of IHCs (Fig. 6*A–C*). To further control for specificity of the antibody, we labeled serial sections with pAb_ΔIQ preabsorbed with GST-fusion protein containing the 27 amino acids and synthetic peptide (Genemed Synthesis) (see Materials and Methods) (Fig. 6*BVII*) or with preimmune serum (Fig. 6*BVIII*). The molar ratio of blocking peptide to antibody was 100:1. In both experiments, the OHCs were not labeled, confirming specificity. For IHCs, only slight pAb_ΔIQ labeling was observed near the apical pole and footplate of nearby pillar cells, and there was no appreciable trend along the frequency gradient of the cochlea. At high magnification, ~100×, the immunolabeling was observed as punctuated dots along the basolateral membrane, cytoplasmic region, and base of the OHCs (Fig. 6*BIX*). Therefore, the localization of such splice variant $Ca_V1.3_{IQ\Delta}$ channels might suggest other processes other than synaptic transmission, perhaps modulating electromotility of the OHCs and regulating events in the lateral wall (Belyantseva et al., 2000; Dallos and Fakler, 2002; Adler et al., 2003).

Because there was a hint of a modest spatial difference in the expression of the $Ca_V1.3_{IQ\Delta}$ channel in the adult (P28), we wondered whether this spatial preference might be more pronounced in sections from younger animals, at a stage in which differential expression of $Ca_V1.3_{IQ\Delta}$ channels might contribute to the activity-dependent sculpting of hair cell development. Electrophysiological studies described the developmental time course of calcium currents in cochlear hair cells, with a peak in magnitude near P9 (Brandt et al., 2003). Thus, we labeled cochlea obtained from P9 rats, for comparison with our foregoing studies at P28. We found again that the three rows of OHCs were strongly labeled, whereas the IHCs were only weakly labeled (Fig. 6*BIV–BVI*), which is not different from the P28 cochlear profile. However, there appeared to be more pronounced expression in basal turns. In contrast, $Ca_V1.3_{IQfull}$ channels appeared to exhibit an inverse preference for IHCs over OHCs. Antibody pAb_$Ca_V1.3$ labeled the IHCs more prominently (Fig. 6*CI*), with lesser signal in OHCs and Deiter's cells. The specificity of pAb_$Ca_V1.3$ labeling was validated by the lack of signals after preabsorption with the corresponding antigenic peptide (Fig. 6*CII*). The molar ratio of blocking peptide to antibody was 100:1.

In all, given the localization of $Ca_V1.3_{IQ\Delta}$ channels within hair cells, the alteration of the IQ motif within these channels represents an attractive molecular basis for much of the weakened CDI

of native currents within OHCs. Our companion paper (Yang et al., 2006) raises the possibility that preferential expression of CaBP4 molecules within IHCs may explain the moderate CDI of native channels in IHCs. Together, these two mechanisms promise to explain the mysteriously weak inactivation phenotype of $Ca_V1.3$ channels in auditory hair cells.

Discussion

In this study, we demonstrated that alternative splicing creates an additional $Ca_V1.3$ channel type ($Ca_V1.3_{IQ\Delta}$) that may underlie the lack of CDI, particularly as observed in outer hair cells. Because the weakly inactivating phenotype of native $Ca_V1.3$ channels is believed critical to hair-cell function, identification of $Ca_V1.3_{IQ\Delta}$ channels represents a potential molecular mechanism underlying the important neurobiological roles subserved by this phenotype. This possibility motivates three topics of discussion: (1) explicit consideration of these neurobiological functions within the auditory context, (2) comparison of the currently known molecular mechanisms for moderating $Ca_V1.3$ inactivation, and (3) the potential for harnessing this molecular knowledge to probe the function of $Ca_V1.3$ CDI *in vivo*.

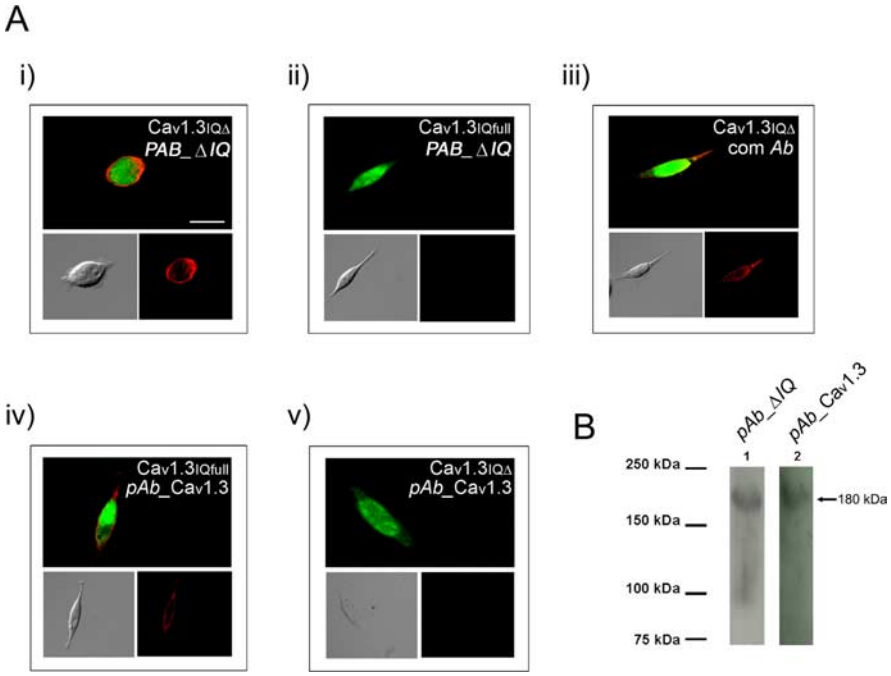

Figure 5. Characterization of pAb_ΔIQ and pAb_$Ca_V1.3$-specific antibodies by immunolabeling and Western blot. ***A***, Specific immunolabeling by pAb_ΔIQ (labeled red with rhodamine-conjugated anti-rabbit IgG) of $Ca_V1.3_{IQ\Delta}$ channels (***i***) expressed on plasma membrane of mammalian HEK293 cells with cotransfected β_{2a} subunits (cytoplasmic) tagged with GFP (green), whereas no plasma membrane labeling is seen on cells cotransfected with $Ca_V1.3_{IQfull}$ and β_{2a} subunits (green; ***ii***). Commercial anti-$Ca_V1.3$ antibody (Alomone Labs; host, rabbit) labeled cells on the plasma membrane (rhodamine-conjugated anti-rabbit IgG) cotransfected with $Ca_V1.3_{IQ\Delta}$ and β_{2a} subunits (green; ***iii***). Similarly, specific immunolabeling by pAb_$Ca_V1.3$ is detected on cells (rhodamine-conjugated anti-rabbit IgG) coexpressing $Ca_V1.3_{IQfull}$ with β_{2a} subunits (green; ***iv***) but not with $Cav1.3_{IQ\Delta}$ (***v***) channels cotransfected with β_{2a} subunits (green). Phase-contrast images of the transfected HEK293 cells were shown in all the panels. ***B***, Presence of $Ca_V1.3_{IQfull}$ and $Ca_V1.3_{IQ\Delta}$ channels in rat cochlear hair cells: Western blot using 20 μg of total membrane protein obtained from rat cochlea was probed with affinity-purified splice variant-specific antibodies. As shown in lanes 1 and 2, labeling by pAb_ΔIQ and pAb_$Ca_V1.3$, respectively, revealed $Ca_V1.3_{IQ\Delta}$ and $Ca_V1.3_{IQfull}$ channel proteins of ~180 kDa in size (indicated by arrow).

Importance of diminished inactivation of $Ca_V1.3$ channels within hair cells

What roles do $Ca_V1.3$ channels that lack CDI serve in auditory outer hair cells? First, minimal CDI of $Ca_V1.3$ channels could sustain persistent $Ca_V1.3$-driven synaptic transmission from outer hair cells to a limited number of afferent nerve connections (Pujol et al., 1997). Second, weak CDI could help prolong Ca^{2+} entry that would sustain activity-dependent transcription underlying outer hair cell development (Platzer et al., 2000; Brandt et al., 2003; Glueckert et al., 2003). During the development of hearing, cochlear hair cells undergo major changes in potassium (Kros et al., 1998; Marcotti et al., 2003) and calcium channel expression (Beutner and Moser, 2001; Michna et al., 2003), as well as dramatic rearrangement of efferent and afferent innervation (Liberman and Simmons, 1985; Sobkowicz et al., 1986, 2004; Simmons and Liberman, 1988a,b; Simmons et al., 1992, 1996; Simmons, 1994, 2002; Fuchs et al., 2003; Bergeron et al., 2005). Hence, the early presence of $Ca_V1.3_{IQ\Delta}$ channels, as well as the loss of OHCs shortly after the onset of hearing in $Ca_V1.3$ knock-out mice (Platzer et al., 2000), cohere with a contribution of these channels to activity-dependent gene expression underlying development. Third, scant inactivation would permit $Ca_V1.3$ channels to sustain voltage-dependent ion-channel effects to expand the "RC frequency limit" of electromotility in outer hair cells, thereby enhancing cochlear amplifier function (Ospeck et al., 2003).

Regarding inner hair cells, $Ca_V1.3_{IQfull}$ channels appear predominant in this locus, with only limited staining for $Ca_V1.3_{IQ\Delta}$ channels. Hence, we believe that another mechanism, involving CaBP4 complexation with $Ca_V1.3_{IQfull}$ channels (Yang et al., 2006), is principally responsible for the weak-to-absent CDI in these hair cells. Accordingly, our companion paper discusses the role of restricted CDI within inner hair cells, and these considerations are not replicated here. Our immunolabeling data differ slightly from those of Hafidi and Dulon (2004). The likely reason is that the antibody (Alomone Labs) used by them recognize the region of antigenic sites located within the II-III intracellular loop. Such an antibody recognizes a common epitope and therefore labels all $Ca_v1.3$ channel splice variants. Our study, however, used two splice variant-specific antibodies, one recognizing the short C terminus form of $Ca_V1.3_{IQfull}$ channels, whereas the other recognizes the splice variant of $Ca_V1.3_{IQ\Delta}$ channels.

Potential mechanisms for switching the inactivation of $Ca_V1.3$ channels in hair cells

There has been a long-standing search for the molecular basis underlying the customized gating properties of hair cell Ca^{2+} currents (Art and Fettiplace, 1987; Zidanic and Fuchs, 1995; Platzer et al., 2000; Schnee and Ricci, 2003). Previous studies proposed that $Ca_V1.3$ splice variants may be involved (Green et al., 1996; Kollmar et al., 1997a,b; Ramakrishnan et al., 2002). In particular, $Ca_V1.3$ of the chicken basilar papilla (Kollmar et al., 1997a,b) has an additional 26 amino acids within the I-II loop region (exon 9a) of $Ca_V1.3$, and the I-II loop has been proposed as a "hinged lid" to obstruct the channel pore and bring about inactivation. Likewise, Song et al. (2003) and others have suggested that muted CDI may partially arise from α_1 subunit association

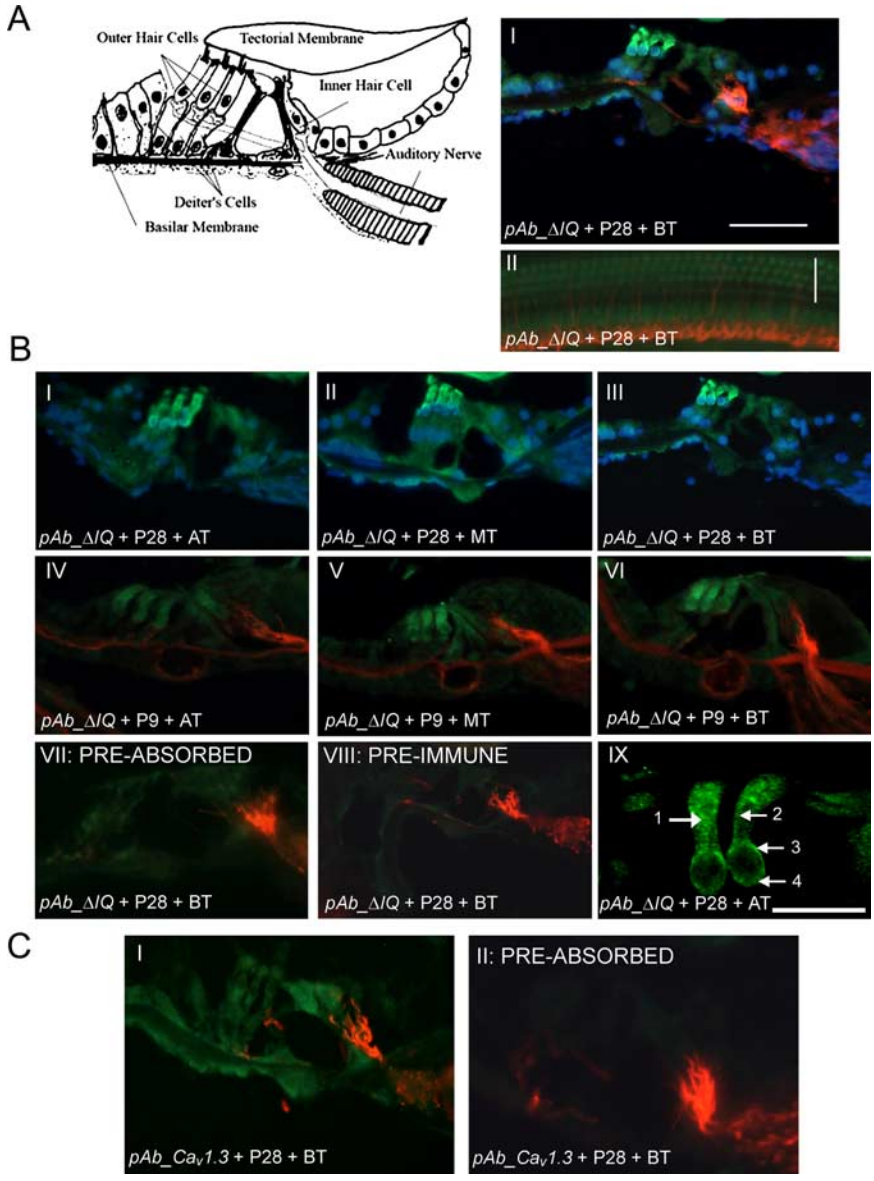

Figure 6. Localization of $Ca_V1.3_{IQ\Delta}$ and $Ca_V1.3_{IQfull}$ channels in rat cochlear hair cells. ***A***, Left, Diagram showing the reference locations of the adult rat cochlear hair cells (P28), supporting cells, basilar, and tectorial membrane and auditory nerve fibers. Right, BT of the adult rat cochlear hair cells immunolabeled with pAb_ΔIQ (***I***; green) shows predominant expression in the OHCs, anti-NF200 (red) immunolabeled the neurofilaments network (afferent fibers), and DAPI staining (blue) indicates the nuclei. The images were merged to demonstrate the localization of the $Ca_V1.3_{IQ\Delta}$ channels on the OHCs. Whole preparations of the cochlear hair cells show that all three rows of the OHCs are intensely immunolabeled by pAb_ΔIQ (***II***) antibody. Scale bars, 20 μm. ***B***, Specific localization and expression patterns of $Ca_V1.3_{IQ\Delta}$ channels in both P9 (before onset of hearing) and P28 cochlear hair cells labeled by pAb_ΔIQ (***I–VI***) on the OHCs. Serial sections of the three turns of P28 cochlear hair cells (AT, apical turn; MT, mid turn; BT) show that all three rows of the OHCs are intensely immunolabeled by pAb_ΔIQ antibody (***I–III***). Localization of $Ca_V1.3_{IQ\Delta}$ channels in young rat cochlear hair cells before the onset of hearing (P9). Three rows of OHCs were strongly labeled, and IHCs were again faintly labeled by the pAb_ΔIQ antibody. All three turns of the young rat cochlear hair cells showed similar labeling patterns. Specificity of the splice variant antibodies was confirmed by the lack of labeling when antibodies preabsorbed with peptide (***VII***) or when preimmune serum (***VIII***) was used. To control for the expression of channels, the BT of the adult rat cochlear hair cells was immunolabeled with pAb_$Ca_V1.3$ channels (***VIII***). The OHCs are magnified 100× under the confocal microscope (***IX***) to reveal the subcellular localization. Cytoplasmic labeling (arrow 1), parts of basolateral membrane (arrow 2), nuclear envelope (arrow 3), and synaptic release sites/base of OHCs (arrow 4) are immunolabeled with pAb_ΔIQ antibody (green). Scale bar, 5 μm. ***C***, $Ca_V1.3_{IQfull}$ channels labeled by pAb_$Ca_V1.3$ channels (***I***) show strong expression on IHCs and weaker expression on the OHC. Specificity of the pAb_$Ca_V1.3$ was confirmed by the lack of labeling when antibodies preabsorbed with peptide (***II***).

with different auxiliary subunits ($\alpha_2\delta$ and β) or presynaptic proteins. Previous reports showed that the mouse cochlea expressed $Ca_V1.2$, $Ca_V1.3$, $Ca_V2.3$, and auxiliary subunits $\alpha_2\delta$, β_1, β_3, and β_4 (Green et al., 1996; Song et al., 2003). The auxiliary subunits when coexpressed with the α_1 subunits modulate the kinetics and properties of channel gating (Lacerda et al., 1991; Singer et al., 1991; Varadi et al., 1991). However, in all of these previous screens, either no explicit functional confirmation of altered CDI was performed (Green et al., 1996; Kollmar et al., 1997a,b; Ramakrishnan et al., 2002), or the blunting of CDI was insufficient to explain the profile of native channels (Song et al., 2003). It has been shown that alternative splicing of the $Ca_V1.2$ gene (Soldatov et al., 1997; Zuhlke and Reuter, 1998; Zuhlke et al., 2000; Tang et al., 2004) contributed to functional diversity of these L-type channels. Previous studies have reported that voltage- or Ca^{2+}-dependent inactivation was influenced by different sites on the $Ca_V1.2$ subunit (Yatani et al., 1994; Parent et al., 1995).

The alternative splicing of the IQ domain in $Ca_V1.3_{IQ\Delta}$ channels as reported here and the complexation of CaBPs with $Ca_V1.3_{IQfull}$ channels described in our companion study (Yang et al., 2006) both provide the first candidate mechanisms whereby the CDI of $Ca_V1.3$ channels is essentially eliminated, consistent with the profile of native channels. The identification of $Ca_V1.3_{IQ\Delta}$ channels adds to a growing list of ion channels customized by alternative splicing (Lin, 1997; Soong et al., 2002; Chaudhuri et al., 2004; Chaudhuri et al., 2005), and the actions of CaBP1/4 on $Ca_V1.3$ channels (Yang et al., 2006) augments an emerging general theme in which CaM-like molecules expand the baseline CaM regulatory profile of various Ca^{2+}-signaling proteins (Burgoyne and Weiss, 2001). Although other molecular explanations may remain to be discovered, it is worth discussing how the present two mechanisms may be integrated within the organ of Corti, as a framework for future work.

In OHCs, the main mechanism for restricting CDI would be the enrichment for $Ca_V1.3_{IQ\Delta}$ channels. Concerning IHCs, the dominant mechanism for limiting inactivation would be the association of $Ca_V1.3_{IQfull}$ channels with CaBP4 molecules. In this setting, there would be a secondary contribution of $Ca_V1.3_{IQ\Delta}$ channels, for which weak staining in IHCs was observed. In our companion study (Yang et al., 2006), we found that both CaBP1 and CaBP4 were capable of eliminating CDI of expression of $Ca_V1.3_{IQfull}$ channels, but that there was preferential expression of only CaBP4 within IHCs. This differential expression pattern of CaBPs suggests different mechanisms for CDI in OHCs versus IHCs.

It is interesting to wonder why different hair cells would use

different mechanisms for eliminating CDI of $Ca_V1.3$ channels. One possibility concerns the potentially different time scales over which CDI is downregulated by the differing mechanisms. In particular, whereas CDI is generally weak to absent in hair cells, there is certainly variability in the extent to which CDI is eliminated among different cells (Michna et al., 2003). Accordingly, the degree of CDI restriction may need to be regulated and thus fine-tuned to cell-specific biological need. There is growing awareness that stability and robustness in Ca^{2+}-signaling networks requires feedback loops that operate on very different time scales (Brandt et al., 2005). An attractive hypothesis, then, is that the time frame over which CDI can be variably throttled may be very different for alternative splicing versus CaBP mechanisms. Channel turnover would predict a time constant of ~1 d for adjusting CDI by alternative splicing (Passafaro et al., 1992). In contrast, CaBPs are capable of binding Ca^{2+}, and their interaction with $Ca_V1.3$ channels may be altered over minutes to hours, according to the recent history of Ca^{2+} elevation (Burgoyne and Weiss, 2001).

Calcium channels in hair cells must maintain a finite level of open probability to support spontaneous activity in associated afferent neurons (Robertson and Paki, 2002): too little and the afferent will fall silent, too much and there will be compression of the synapse's dynamic range. Therefore, it is likely that interacting molecular mechanisms are used to ensure an appropriate level of activity. Slow CDI serves as negative feedback, adjusting open probability to the ongoing calcium flux. In turn, the efficacy of CDI will depend on the presence of $Ca_V1.3_{IQ\Delta}$ splice variants and (in inner hair cells) modulation by calmodulin-like calcium-binding proteins. Therefore, CDI is not involved in channel gating at acoustic frequencies. Rather, CDI adjusts "steady-state" open probability to comply with prolonged changes in net activity.

Tools for *in vivo* dissection of $Ca_V1.3$ function in hair cells

Overall, the discovery of candidate molecular explanations for the diminished CDI of native auditory currents, alternative-splicing ($Ca_V1.3_{IQ\Delta}$ channels, described here) and CaBP interactions (Yang et al., 2006), promises the groundwork for exploring the neuroauditory impact of CDI regulation *in vivo*. Transgenic animal models with a splice variant-specific knock-out of $Ca_V1.3_{IQ\Delta}$ channels, or with selective elimination of CaBP4 expression (Haeseleer et al., 2004), could permit direct exploration of the auditory signaling role of sustained $Ca_V1.3$ channel activity within outer versus inner hair cells, respectively. Alternatively, RNA silencing or expression of CaBP "buffer" molecules within the *in vivo* context could also prove useful. Experiments using such strategies now present as promising arenas for future research.

References

Adler HJ, Belyantseva IA, Merritt Jr RC, Frolenkov GI, Dougherty GW, Kachar B (2003) Expression of prestin, a membrane motor protein, in the mammalian auditory and vestibular periphery. Hear Res 184:27–40.

Art JJ, Fettiplace R (1987) Variation of membrane properties in hair cells isolated from the turtle cochlea. J Physiol (Lond) 385:207–242.

Belyantseva IA, Adler HJ, Curi R, Frolenkov GI, Kachar B (2000) Expression and localization of prestin and the sugar transporter GLUT-5 during development of electromotility in cochlear outer hair cells. J Neurosci 20:RC116(1–5).

Bergeron AL, Schrader A, Yang D, Osman AA, Simmons DD (2005) The final stage of cholinergic differentiation occurs below inner hair cells during development of the rodent cochlea. J Assoc Res Otolaryngol 1–15.

Beutner D, Moser T (2001) The presynaptic function of mouse cochlear inner hair cells during development of hearing. J Neurosci 21:4593–4599.

Brandt A, Striessnig J, Moser T (2003) $Ca_V1.3$ channels are essential for development and presynaptic activity of cochlear inner hair cells. J Neurosci 23:10832–10840.

Brandt A, Khimich D, Moser T (2005) Few $Ca_V1.3$ channels regulate the exocytosis of a synaptic vesicle at the hair cell ribbon synapse. J Neurosci 25:11577–11585.

Brownell WE, Bertrand D, de Ribaupierre Y (1985) Evoked mechanical responses of isolated cochlear outer hair cells. Science 227:194–196.

Burgoyne RD, Weiss JL (2001) The neuronal calcium sensor family of Ca2+-binding proteins. Biochem J 353:1–12.

Cens T, Rousset M, Leyris JP, Fesquet P, Charnet P (2006) Voltage- and calcium-dependent inactivation in high voltage-gated Ca(2+) channels. Prog Biophys Mol Biol 90:104–117.

Chaudhuri D, Chang SY, DeMaria CD, Alvania RS, Soong TW, Yue DT (2004) Alternative splicing as a molecular switch for Ca^{2+}/calmodulin-dependent facilitation of P/Q-type Ca^{2+} channels. J Neurosci 24:6334–6342.

Chaudhuri D, Alseikhan BA, Chang SY, Soong TW, Yue DT (2005) Developmental activation of calmodulin-dependent facilitation of cerebellar P-type Ca^{2+} current. J Neurosci 25:8282–8294.

Dallos P, Fakler B (2002) Prestin, a new type of motor protein. Nat Rev Mol Cell Biol 3:104–111.

DeMaria CD, Soong TW, Alseikhan BA, Alvania RS, Yue DT (2001) Calmodulin bifurcates the local Ca2+ signal that modulates P/Q-type Ca2+ channels. Nature 411:484–489.

Fuchs PA (1996) Synaptic transmission at vertebrate hair cells. Curr Opin Neurobiol 6:514–519.

Fuchs PA, Nagai T, Evans MG (1988) Electrical tuning in hair cells isolated from the chick cochlea. J Neurosci 8:2460–2467.

Fuchs PA, Evans MG, Murrow BW (1990) Calcium currents in hair cells isolated from the cochlea of the chick. J Physiol (Lond) 429:553–568.

Fuchs PA, Glowatzki E, Moser T (2003) The afferent synapse of cochlear hair cells. Curr Opin Neurobiol 13:452–458.

Gao T, Bunemann M, Gerhardstein BL, Ma H, Hosey MM (2000) Role of the C terminus of the alpha 1C (CaV1.2) subunit in membrane targeting of cardiac L-type calcium channels. J Biol Chem 275:25436–25444.

Glossmann H, Striessnig J, Ferry DR, Goll A, Moosburger K, Schirmer M (1987) Interaction between calcium channel ligands and calcium channels. Circ Res 61:I30–I36.

Glueckert R, Wietzorrek G, Kammen-Jolly K, Scholtz A, Stephan K, Striessnig J, Schrott-Fischer A (2003) Role of class D L-type Ca2+ channels for cochlear morphology. Hear Res 178:95–105.

Green GE, Khan KM, Beisel DW, Drescher MJ, Hatfield JS, Drescher DG (1996) Calcium channel subunits in the mouse cochlea. J Neurochem 67:37–45.

Haeseleer F, Imanishi Y, Maeda T, Possin DE, Maeda A, Lee A, Rieke F, Palczewski K (2004) Essential role of Ca2+-binding protein 4, a Cav1.4 channel regulator, in photoreceptor synaptic function. Nat Neurosci 7:1079–1087.

Hafidi A, Dulon D (2004) Developmental expression of Ca(v)1.3 (alpha1d) calcium channels in the mouse inner ear. Brain Res Dev Brain Res 150:167–175.

Helton TD, Xu W, Lipscombe D (2005) Neuronal L-type calcium channels open quickly and are inhibited slowly. J Neurosci 25:10247–10251.

Hudspeth AJ, Lewis RS (1988) A model for electrical resonance and frequency tuning in saccular hair cells of the bull-frog, *Rana catesbeiana*. J Physiol (Lond) 400:275–297.

Jiang GJ, Zidanic M, Michaels RL, Michael TH, Griguer C, Fuchs PA (1997) CSlo encodes calcium-activated potassium channels in the chick's cochlea. Proc Biol Sci 264:731–737.

Jones EM, Laus C, Fettiplace R (1998) Identification of Ca(2+)-activated K+ channel splice variants and their distribution in the turtle cochlea. Proc Biol Sci 265:685–692.

Kollmar R, Montgomery LG, Fak J, Henry LJ, Hudspeth AJ (1997a) Predominance of the alpha1D subunit in L-type voltage-gated Ca2+ channels of hair cells in the chicken's cochlea. Proc Natl Acad Sci USA 94:14883–14888.

Kollmar R, Fak J, Montgomery LG, Hudspeth AJ (1997b) Hair cell-specific splicing of mRNA for the alpha1D subunit of voltage-gated Ca2+ channels in the chicken's cochlea. Proc Natl Acad Sci USA 94:14889–14893.

Kros CJ, Ruppersberg JP, Rusch A (1998) Expression of a potassium current

in inner hair cells during development of hearing in mice. Nature 394:281–284.
Lacerda AE, Kim HS, Ruth P, Perez-Reyes E, Flockerzi V, Hofmann F, Birnbaumer L, Brown AM (1991) Normalization of current kinetics by interaction between the alpha 1 and beta subunits of the skeletal muscle dihydropyridine-sensitive Ca2+ channel. Nature 352:527–530.
Lewis RS, Hudspeth AJ (1983) Voltage- and ion-dependent conductances in solitary vertebrate hair cells. Nature 304:538–541.
Liang H, DeMaria CD, Erickson MG, Mori MX, Alseikhan BA, Yue DT (2003) Unified mechanisms of Ca2+ regulation across the Ca2+ channel family. Neuron 39:951–960.
Liberman MC, Simmons DD (1985) Applications of neuronal labeling techniques to the study of the peripheral auditory system. J Acoust Soc Am 78:312–319.
Lin X (1997) Action potentials and underlying voltage-dependent currents studied in cultured spiral ganglion neurons of the postnatal gerbil. Hear Res 108:157–179.
Marcotti W, Johnson SL, Rusch A, Kros CJ (2003) Sodium and calcium currents shape action potentials in immature mouse inner hair cells. J Physiol (Lond) 552:743–761.
Michna M, Knirsch M, Hoda JC, Muenkner S, Langer P, Platzer J, Striessnig J, Engel J (2003) Cav1.3 (alpha1D) Ca2+ currents in neonatal outer hair cells of mice. J Physiol (Lond) 553:747–758.
Navaratnam DS, Bell TJ, Tu TD, Cohen EL, Oberholtzer JC (1997) Differential distribution of Ca2+-activated K+ channel splice variants among hair cells along the tonotopic axis of the chick cochlea. Neuron 19:1077–1085.
Ospeck M, Dong XX, Iwasa KH (2003) Limiting frequency of the cochlear amplifier based on electromotility of outer hair cells. Biophys J 84:739–749.
Parent L, Gopalakrishnan M, Lacerda AE, Wei X, Perez-Reyes E (1995) Voltage-dependent inactivation in a cardiac-skeletal chimeric calcium channel. FEBS Lett 360:144–150.
Parsons TD, Lenzi D, Almers W, Roberts WM (1994) Calcium-triggered exocytosis and endocytosis in an isolated presynaptic cell: capacitance measurements in saccular hair cells. Neuron 13:875–883.
Passafaro M, Clementi F, Sher E (1992) Metabolism of omega-conotoxin-sensitive voltage-operated calcium channels in human neuroblastoma cells: modulation by cell differentiation and anti-channel antibodies. J Neurosci 12:3372–3379.
Patil PG, Brody DL, Yue DT (1998) Preferential closed-state inactivation of neuronal calcium channels. Neuron 20:1027–1038.
Peterson BZ, DeMaria CD, Adelman JP, Yue DT (1999) Calmodulin is the Ca2+ sensor for Ca2+ -dependent inactivation of L-type calcium channels. Neuron 22:549–558.
Peterson BZ, Lee JS, Mulle JG, Wang Y, de Leon M, Yue DT (2000) Critical determinants of Ca(2+)-dependent inactivation within an EF-hand motif of L-type Ca(2+) channels. Biophys J 78:1906–1920.
Platzer J, Engel J, Schrott-Fischer A, Stephan K, Bova S, Chen H, Zheng H, Striessnig J (2000) Congenital deafness and sinoatrial node dysfunction in mice lacking class D L-type Ca2+ channels. Cell 102:89–97.
Pujol R, Lavigne-rebillard M, Lenoir M (1997) Development of sensory and neural structures in the mammalian cochlea. In: Development of the auditory system, Springer handbook of auditory research (Fay RR, ed), pp 156–192. New York: Springer.
Ramakrishnan NA, Green GE, Pasha R, Drescher MJ, Swanson GS, Perin PC, Lakhani RS, Ahsan SF, Hatfield JS, Khan KM, Drescher DG (2002) Voltage-gated Ca2+ channel Ca(V)1.3 subunit expressed in the hair cell epithelium of the sacculus of the trout *Oncorhynchus mykiss*: cloning and comparison across vertebrate classes. Brain Res Mol Brain Res 109:69–83.
Robertson D, Paki B (2002) Role of L-type Ca2+ channels in transmitter release from mammalian inner hair cells. II. Single-neuron activity. J Neurophysiol 87:2734–2740.
Rodriguez-Contreras A, Yamoah EN (2001) Direct measurement of single-channel Ca(2+) currents in bullfrog hair cells reveals two distinct channel subtypes. J Physiol (Lond) 534:669–689.
Rosenblatt KP, Sun ZP, Heller S, Hudspeth AJ (1997) Distribution of Ca2+-activated K+ channel isoforms along the tonotopic gradient of the chicken's cochlea. Neuron 19:1061–1075.
Schnee ME, Ricci AJ (2003) Biophysical and pharmacological characterization of voltage-gated calcium currents in turtle auditory hair cells. J Physiol (Lond) 549:697–717.
Simmons DD (1994) A transient afferent innervation of outer hair cells in the postnatal cochlea. NeuroReport 5:1309–1312.
Simmons DD (2002) Development of the inner ear efferent system across vertebrate species. J Neurobiol 53:228–250.
Simmons DD, Liberman MC (1988a) Afferent innervation of outer hair cells in adult cats: I. Light microscopic analysis of fibers labeled with horseradish peroxidase. J Comp Neurol 270:132–144.
Simmons DD, Liberman MC (1988b) Afferent innervation of outer hair cells in adult cats: II. Electron microscopic analysis of fibers labeled with horseradish peroxidase. J Comp Neurol 270:145–154.
Simmons DD, Bertolotto C, Narins PM (1992) Innervation of the amphibian and basilar papillae in the leopard frog: reconstructions of single labeled fibers. J Comp Neurol 322:191–200.
Simmons DD, Mansdorf NB, Kim JH (1996) Olivocochlear innervation of inner and outer hair cells during postnatal maturation: evidence for a waiting period. J Comp Neurol 370:551–562.
Singer D, Biel M, Lotan I, Flockerzi V, Hofmann F, Dascal N (1991) The roles of the subunits in the function of the calcium channel. Science 253:1553–1557.
Sobkowicz HM, Rose JE, Scott GL, Levenick CV (1986) Distribution of synaptic ribbons in the developing organ of Corti. J Neurocytol 15:693–714.
Sobkowicz HM, August BK, Slapnick SM (2004) Synaptic arrangements between inner hair cells and tunnel fibers in the mouse cochlea. Synapse 52:299–315.
Soldatov NM, Zuhlke RD, Bouron A, Reuter H (1997) Molecular structures involved in L-type calcium channel inactivation. Role of the carboxyl-terminal region encoded by exons 40–42 in alpha1C subunit in the kinetics and Ca2+ dependence of inactivation. J Biol Chem 272:3560–3566.
Song H, Nie L, Rodriguez-Contreras A, Sheng ZH, Yamoah EN (2003) Functional interaction of auxiliary subunits and synaptic proteins with Ca(v)1.3 may impart hair cell Ca2+ current properties. J Neurophysiol 89:1143–1149.
Soong TW, DeMaria CD, Alvania RS, Zweifel LS, Liang MC, Mittman S, Agnew WS, Yue DT (2002) Systematic identification of splice variants in human P/Q-type channel α1(2.1) subunits: implications for current density and Ca^{2+}-dependent inactivation. J Neurosci 22:10142–10152.
Tang ZZ, Liang MC, Lu S, Yu D, Yu CY, Yue DT, Soong TW (2004) Transcript scanning reveals novel and extensive splice variations in human l-type voltage-gated calcium channel, Cav1.2 alpha1 subunit. J Biol Chem 279:44335–44343.
Varadi G, Lory P, Schultz D, Varadi M, Schwartz A (1991) Acceleration of activation and inactivation by the beta subunit of the skeletal muscle calcium channel. Nature 352:159–162.
Xu W, Lipscombe D (2001) Neuronal $Ca_V1.3\alpha(1)$ L-type channels activate at relatively hyperpolarized membrane potentials and are incompletely inhibited by dihydropyridines. J Neurosci 21:5944–5951.
Yatani A, Bahinski A, Wakamori M, Tang S, Mori Y, Kobayashi T, Schwartz A (1994) Alteration of channel characteristics by exchange of pore-forming regions between two structurally related Ca2+ channels. Mol Cell Biochem 140:93–102.
Yue DT, Marban E (1990) Permeation in the dihydropyridine-sensitive calcium channel. Multi-ion occupancy but no anomalous mole-fraction effect between Ba2+ and Ca2+. J Gen Physiol 95:911–939.
Zidanic M, Fuchs PA (1995) Kinetic analysis of barium currents in chick cochlear hair cells. Biophys J 68:1323–1336.
Zuhlke RD, Reuter H (1998) Ca2+-sensitive inactivation of L-type Ca2+ channels depends on multiple cytoplasmic amino acid sequences of the alpha1C subunit. Proc Natl Acad Sci USA 95:3287–3294.
Zuhlke RD, Pitt GS, Tsien RW, Reuter H (2000) Ca2+-sensitive inactivation and facilitation of L-type Ca2+ channels both depend on specific amino acid residues in a consensus calmodulin-binding motif in the(alpha)1C subunit. J Biol Chem 275:21121–21129.